

# Gravitational waves from eccentric compact binaries: Reduction in signal-to-noise ratio due to nonoptimal signal processing

Karl Martel and Eric Poisson

*Department of Physics, University of Guelph, Guelph, Ontario, Canada N1G 2W1*

## Abstract

Inspiring compact binaries have been identified as one of the most promising sources of gravitational waves for interferometric detectors. Most of these binaries are expected to have circularized by the time their gravitational waves enter the instrument's frequency band. However, the possibility that some of the binaries might still possess a significant eccentricity is not excluded. We imagine a situation in which eccentric signals are received by the detector but not explicitly searched for in the data analysis, which uses exclusively circular waveforms as matched filters. We ascertain the likelihood that these filters, though not optimal, will nevertheless be successful at capturing the eccentric signals. We do this by computing the loss in signal-to-noise ratio incurred when searching for eccentric signals with those nonoptimal filters. We show that for a binary system of a given total mass, this loss increases with increasing eccentricity. We show also that for a given eccentricity, the loss decreases as the total mass is increased.

Pacs numbers: 04.25.Nx; 04.30.Db; 04.80.Nn

arXiv:gr-qc/9907006v2 30 Aug 1999

Typeset using REVTeX

## I. INTRODUCTION AND SUMMARY

Gravitational waves produced during the last few minutes of inspiral of compact binary systems — composed of neutron stars and/or black holes — are among the most promising for detection by kilometer-size interferometric detectors such as LIGO, VIRGO, GEO600, and TAMA. The ongoing construction of these instruments has prompted many workers to develop strategies to search for eventual inspiraling-binary signals in the noisy data streams [1–18]. The main idea is to use the well-known technique of matched filtering [19] to help find a gravitational-wave signal that may be deeply buried in detector noise. This technique consists of cross-correlating the detector output with a set of model waveforms (often called templates) which depend on a number of parameters characterizing the source. These parameters are varied until the signal-to-noise ratio is maximized, and a signal is concluded to be present — within a certain degree of confidence — if the signal-to-noise ratio exceeds a certain threshold. Within the class of linear filtering methods, matched filtering is known to be optimal [19] when the model waveform which maximizes the signal-to-noise ratio is an accurate representation of the actual signal. The development of templates that are sufficiently accurate for the detection of inspiraling-binary signals is currently a very active area of research.

In this continuing effort to generate accurate templates, it is usually assumed that the binary system moves on a sequence of circular orbits, with the orbital radius decreasing slowly as a result of radiation reaction. For most compact binaries, this *quasi-circular* approximation is well justified, because radiation reaction decreases the orbital eccentricity as the system evolves toward smaller orbits [20]. If  $a$  and  $e$  respectively denote the binary's semi-major axis and eccentricity, then radiation reaction changes these quantities according to the approximate relation  $e/e_0 \simeq (a/a_0)^{19/12}$ ;  $a_0$  and  $e_0$  are the initial values [20]. This relation implies that a reduction in semi-major axis by a factor of 2 comes with a reduction in eccentricity by a factor of approximately 3. Thus, radiation reaction quickly circularizes the orbit, and any long-lived compact binary, of the sort produced when an ordinary (but massive) binary star reaches the endpoint of stellar evolution, will have become circular by the time its gravitational waves become measurable. (To be measurable, the waves must have a frequency that lies within the detector's frequency band, between 40 Hz and 1000 Hz for the initial LIGO detector. The dominant contribution to the waves comes at twice the orbital frequency. Thus, the waves enter the relevant frequency band when the orbital frequency becomes larger than 20 Hz. For a binary system consisting of two neutron stars, each of 1.4 solar masses, this corresponds to an orbital radius of 290 km and an orbital velocity of  $0.12c$ , where  $c$  is the speed of light.)

While probably most binaries will have become circular by the time their gravitational waves enter the frequency band of interferometric detectors, the possibility that some binaries might still have a significant eccentricity is not excluded. The formation scenario for these eccentric binaries is different from what was considered in the preceding paragraph. We may imagine that in a densely populated region of the universe, such as the core of a globular cluster or the nucleus of a galaxy, a significant number of compact binaries are produced by two- and three-body processes involving initially isolated compact objects. Such a scenario may play an important role in the formation of massive black holes in galactic nuclei [21,22], and it might well provide an interesting number of gravitational-wave sources. Be-

cause some of the resulting binaries will not have time to eliminate their eccentricities before their gravitational waves enter the relevant frequency band, it is conceivable that eccentric compact binaries will make up a sizable fraction of the total number of gravitational-wave sources.

Admitting this possibility, the issue arises as to how this might affect the data-analysis strategies. While it is possible to include the eccentricity in the list of template parameters, doing so would significantly increase the number of templates required to search for signals [11,17]. This would come with an increased computational burden associated with data processing, and a higher setting for the threshold value of the signal-to-noise ratio. On the other hand, using only quasi-circular templates might prevent us from detecting a potentially interesting number of sources, those corresponding to eccentric binaries.

To settle the issue requires information from two fronts. First, we need a reliable estimate of the number of eccentric binaries that might be measured by interferometric detectors in the course of a year. Second, we need to compute the loss of event rate that is incurred when searching for eccentric signals using nonoptimal, circular templates. On the basis of this information we could decide whether an optimal search for eccentric binaries would be worthwhile, even at the price of a higher threshold and increased computational burden, or whether the circular templates would be sufficiently effective at capturing most of the signals, both circular and eccentric.

Our purpose in this paper is to examine the second question, namely, to estimate the loss of event rate incurred when searching for eccentric signals using a nonoptimal set of circular templates. Our main tool in this work is Apostolatos' fitting factor (FF) [8], which measures the degree of optimality of a given set of templates. More concretely, the fitting factor is the ratio of the *actual* signal-to-noise ratio, obtained when searching for eccentric signals using circular templates, to the signal-to-noise ratio that would be obtained if eccentric templates were used instead. A fitting factor close to unity indicates that the circular templates are quite effective at capturing an eccentric signal, and that little would be gained by using an optimal set of templates. On the other hand, a fitting factor much smaller than unity indicates that the circular templates do poorly, and that a set of eccentric templates would be required for a successful search. The loss in event rate caused by using nonoptimal templates is given in terms of the fitting factor by  $1 - \text{FF}^3$ .

The fitting factor is computed as follows [8]. Let  $s(t)$  be the actual gravitational-wave signal corresponding to an eccentric compact binary, and let  $h(t; \boldsymbol{\theta})$  denote the circular templates, with the vector  $\boldsymbol{\theta}$  representing the template parameters. We denote the Fourier transform of these functions by  $\tilde{s}(f)$  and  $\tilde{h}(f; \boldsymbol{\theta})$ , respectively; for any function  $a(t)$ ,  $\tilde{a}(f) = \int_{-\infty}^{\infty} a(t)e^{2\pi ift} dt$ . We first define the ambiguity function  $\mathcal{A}(\boldsymbol{\theta})$  by

$$\mathcal{A}(\boldsymbol{\theta}) = \frac{(s|h)}{\sqrt{(s|s)(h|h)}}, \quad (1)$$

where

$$(a|b) = 2 \int_0^{\infty} \frac{\tilde{a}^*(f)\tilde{b}(f) + \tilde{a}(f)\tilde{b}^*(f)}{S_n(f)} df \quad (2)$$

is the natural matched-filtering inner product. Here, an asterisk denotes complex conjugation and  $S_n(f)$  is the (one-sided) spectral density of the detector noise. For the purpose of

this work we choose a noise curve that roughly mimics the expected noise spectrum of the initial LIGO detector, and set [5]

$$S_n(f) = S_0 \left[ (f_0/f)^4 + 2 + 2(f/f_0)^2 \right] \quad (3)$$

for  $f > 40$  Hz, with  $f_0 = 200$  Hz. The value of  $S_0$  is irrelevant for our purposes, and we take  $S_n(f)$  to be infinite below 40 Hz. The fitting factor is the maximum value of the ambiguity function,

$$\text{FF} = \max_{\boldsymbol{\theta}} \mathcal{A}(\boldsymbol{\theta}), \quad (4)$$

where the maximization is over all possible choices of source parameters.

Expressions for  $s(t)$  and  $\tilde{h}(f; \boldsymbol{\theta})$  will be provided in Sec. II and III, respectively. These expressions are based upon the rather severe assumptions that the binary’s orbital motion is governed by Newtonian gravity, and the adiabatic evolution of the orbital elements governed by the Einstein quadrupole formula. Our waveforms will therefore be left at the “Newtonian” level, and we shall ignore all post-Newtonian corrections to the waveforms. While this level of approximation does not produce a fully realistic waveform, it should nevertheless be sufficient for the purposes of this investigation. A more accurate version of our calculations, based on (say) second post-Newtonian waveforms [23,24], would be technically more difficult; for example, the number of template parameters would have to be increased from 3 to at least 4. In any event, it is doubtful that any of our conclusions would be invalidated by a more sophisticated treatment; we shall come back to this point in Sec. IV.

The ambiguity function and fitting factor are computed in Sec. III. For a given binary system, characterized by a choice of individual masses, the fitting factor is a function of the degree of eccentricity of the orbital motion. Because the eccentricity evolves as the system emits gravitational waves, we must find a meaningful way of parameterizing this. We proceed as follows. We begin the orbital evolution just before the gravitational waves enter the detector’s frequency band. Because the waves have a frequency component at three times the orbital frequency (see Sec. II), this means that we must begin when  $f_{\text{orb}} = 13.3$  Hz, where  $f_{\text{orb}} = (2\pi M)^{-1}(M/a)^{3/2}$  is the orbital frequency. Here,  $M$  denotes the total mass of the binary system and  $a$  is the semi-major axis; we use geometrized units in which  $G = c = 1$ . Having thus specified  $a_0$ , the initial value of the first orbital element, we next choose  $e_0$ , the initial value of the eccentricity. Thus,  $e_0$  is the binary’s eccentricity at the time the gravitational waves enter the instrument’s frequency band. For a given binary system, we take FF to be a function of  $e_0$ .

This function is plotted for selected binaries in Fig. 1. While  $\text{FF} = 1$  when  $e_0 = 0$ , we see that the fitting factor decreases monotonically as  $e_0$  increases. This was to be expected: As the eccentricity increases, the circular templates become less effective at capturing the gravitational-wave signal. We also see that FF decreases faster for small-mass binaries than it does for large-mass binaries. As we shall see in Sec. II, this has to do with the fact that the gravitational-wave signal is shorter for large-mass systems, so that the circular templates have less of an opportunity to go out of phase.

If we select a cutoff  $\text{FF}|_{\text{min}}$  for the fitting factor, dismissing as inadequate those templates for which  $\text{FF} < \text{FF}|_{\text{min}}$ , we see that the range of eccentricities for which the circular templates are adequate increases with the total mass of the binary system. For example, let  $\text{FF}|_{\text{min}} =$

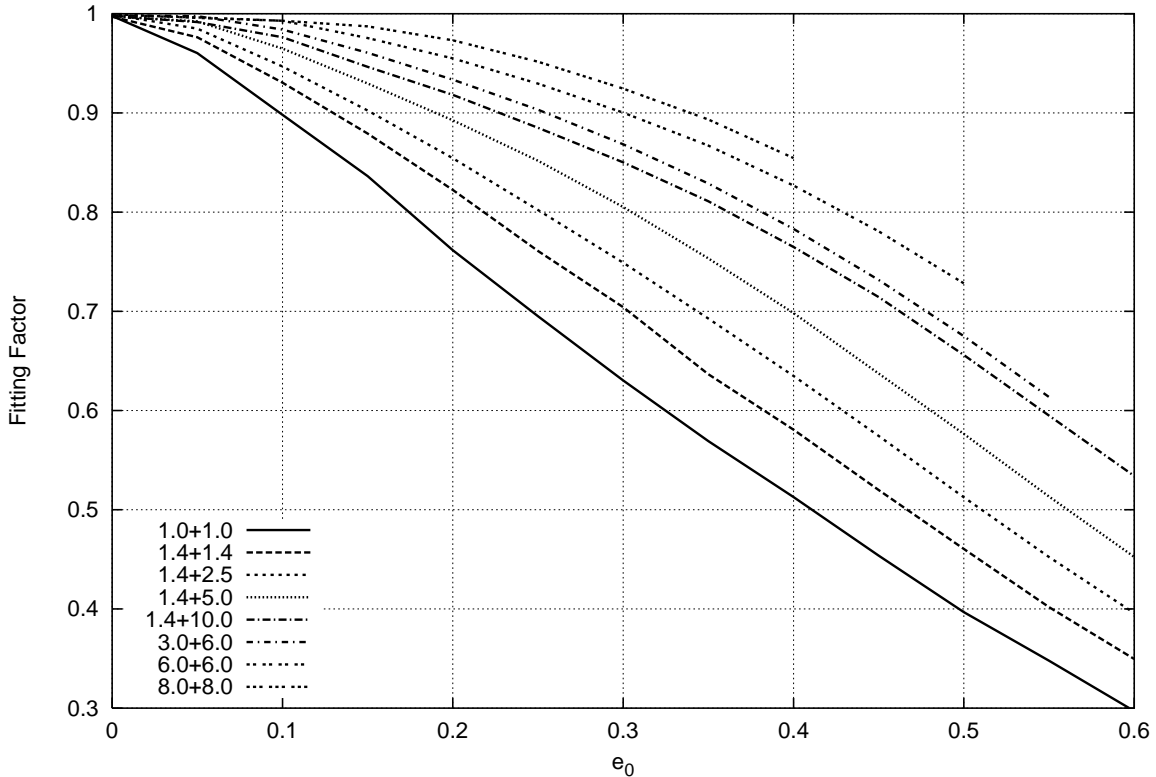


FIG. 1. The fitting factor as a function of initial eccentricity, for selected binary systems. The curves are labelled by the value of the individual masses, given in units of the solar mass.

90%, so that the tolerated loss in event rate is less than 27%. For a binary system consisting of two 1.4 solar-mass neutron stars, the allowed range of eccentricities is  $e_0 \lesssim 0.13$ . For a system of two 6.0 solar-mass black holes, the range is  $e_0 \lesssim 0.30$ . We conclude that an eccentric binary system has a better chance of being detected if it is more massive. This conclusion is reinforced by the fact that massive binaries also emit stronger waves [16]. These observations summarize the results of our investigation.

## II. GRAVITATIONAL WAVES FROM ECCENTRIC BINARIES

The gravitational waves emitted by an eccentric binary system are calculated to leading order in a post-Newtonian expansion. In this approximation, the orbital motion is governed by Newtonian gravity, so that the (relative) orbit is an ordinary Keplerian ellipse. The waves are computed on the basis of the Einstein quadrupole formula, and the adiabatic evolution of the orbital elements is incorporated by taking into account the loss of orbital energy and angular momentum to the gravitational waves. The waveforms were first calculated by Wahlquist [25], and our expressions below are identical to his except for a different notation. The evolution of the orbital elements was first calculated by Peters [20]. Post-Newtonian corrections to these results were recently obtained by Gopakumar and Iyer [24]; their paper contains the foundations for an improved version of our work.

We place the orbit in the  $x$ - $y$  plane of a Cartesian coordinate system, and orient the major axis along the  $x$  axis. The orbital radius is expressed as

$$r = \frac{p M}{1 + e \cos \Phi}, \quad (5)$$

where  $M = m_1 + m_2$  is the total mass,  $p$  a dimensionless semi-latus rectum,  $e$  the eccentricity, and  $\Phi$  the orbital phase, obtained by integrating

$$\frac{d\Phi}{dt} = \frac{(1 + e \cos \Phi)^2}{p^{3/2} M}. \quad (6)$$

The orbital period is given by

$$P = 2\pi M \left( \frac{p}{1 - e^2} \right)^{3/2}, \quad (7)$$

and the semi-major axis is related to  $p$  and  $e$  by  $a = pM/(1 - e^2)$ .

The orbital elements  $p$  and  $e$  both decrease as a function of time by virtue of the fact that the gravitational waves remove energy and angular momentum from the system. The relevant expressions are [20]

$$\frac{dp}{dt} = -\frac{64}{5} \frac{\mu}{M^2} \frac{(1 - e^2)^{3/2}}{p^3} \left( 1 + \frac{7}{8} e^2 \right) \quad (8)$$

and

$$\frac{de}{dt} = -\frac{304}{15} \frac{\mu}{M^2} \frac{(1 - e^2)^{3/2}}{p^4} e \left( 1 + \frac{121}{304} e^2 \right), \quad (9)$$

where  $\mu = m_1 m_2 / (m_1 + m_2)$  is the reduced mass. Equations (6), (8), and (9) determine the orbital motion completely once initial values are provided for  $p$ ,  $e$ , and  $\Phi$ . We shall return to this point below.

We place the gravitational-wave detector at a distance  $R$  from the source, in a direction characterized by the polar angles  $\iota$  and  $\beta$  relative to the Cartesian frame [1]. If we choose  $\hat{\iota}$  and  $\hat{\beta}$  as polarization axes, the two fundamental polarizations of the gravitational waves are [25]

$$s_+ = -\frac{\mu}{pR} \left\{ \left[ 2 \cos(2\Phi - 2\beta) + \frac{5e}{2} \cos(\Phi - 2\beta) + \frac{e}{2} \cos(3\Phi - 2\beta) + e^2 \cos(2\beta) \right] (1 + \cos^2 \iota) + \left[ e \cos(\Phi) + e^2 \right] \sin^2 \iota \right\} \quad (10)$$

and

$$s_\times = -\frac{\mu}{pR} \left[ 4 \sin(2\Phi - 2\beta) + 5e \sin(\Phi - 2\beta) + e \sin(3\Phi - 2\beta) - 2e^2 \sin(2\beta) \right] \cos \iota. \quad (11)$$

Once Eqs. (6), (8), and (9) have been integrated, the waveforms can easily be computed. Inspection of Eqs. (10) and (11) reveals that the gravitational waves can be decomposed into components that oscillate at once, twice, and three times the orbital frequency  $f_{\text{orb}} = 1/P$ . (The wave spectrum is actually more complicated than this because the angular velocity

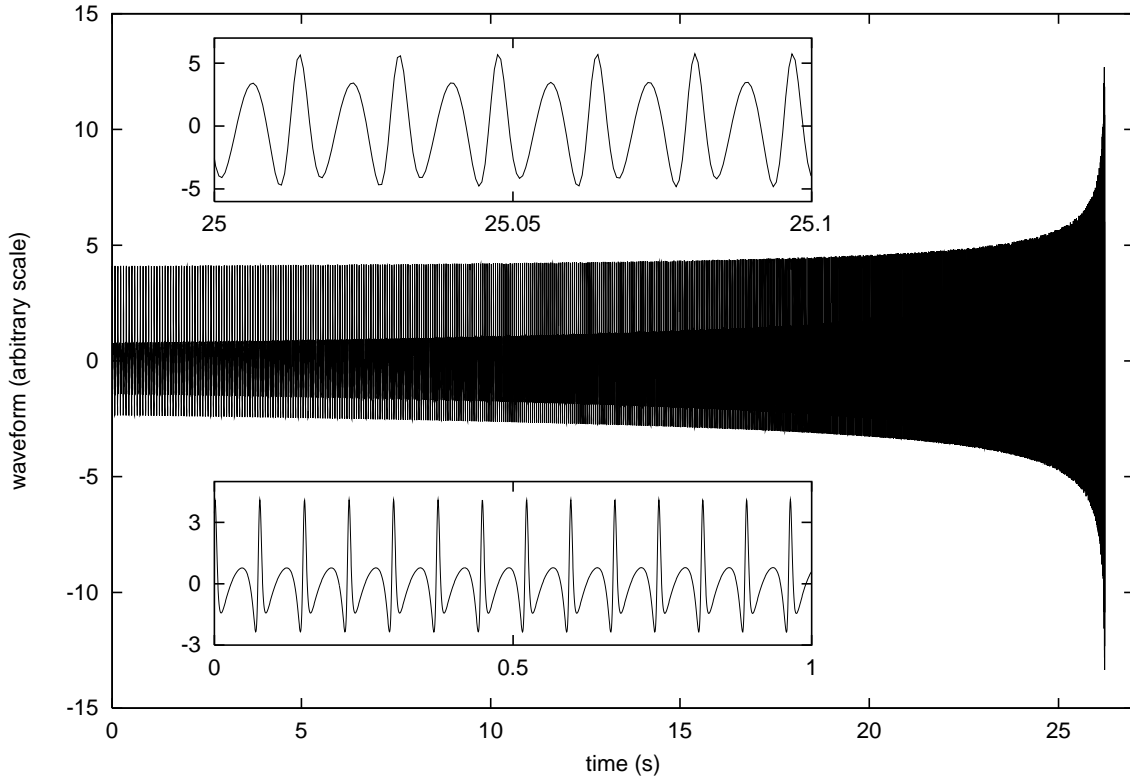


FIG. 2. Plots of  $s(t)$  (up to an overall scaling) for a  $1.4 + 1.4$  binary system with initial eccentricity  $e_0 = 0.5$ . The main figure shows the waveform for its entire duration. The bottom inset shows the waveform at early times, when the eccentricity is still large. The top inset shows the waveform at late times, when the eccentricity is much reduced. Notice the monotonic increase of both the amplitude and frequency.

$d\Phi/dt$  is not uniform. Nevertheless, this decomposition of the waves into three components is still meaningful and useful.) The detector responds to the linear combination  $s(t) = f_+ s_+(t) + f_\times s_\times(t)$ , where  $f_+$  and  $f_\times$  are the detector's beam factors [1]. Our calculations are not sensitive to the numerical value of the beam factors; we choose  $f_+ = 1$  and  $f_\times = 0$ , so that  $s(t) = s_+(t)$ . Similarly, our calculations are not sensitive to the numerical value of  $\iota$  and  $\beta$ ; we choose  $\iota = \pi/4$  and  $\beta = 0$ .

We assume that the gravitational-wave signal began before the waves entered the frequency band of our detector. In our computations, it is sufficient to start the signal immediately before it enters this band. We shall denote by  $f_{\min}$  the lower end of the instrument's frequency band; for the initial version of the LIGO detector,  $f_{\min} = 40$  Hz. The signal component that first enters the band is the one that oscillates at three times the orbital frequency. We must therefore impose  $3f_{\text{orb}} < f_{\min}$  to ensure that our simulated signal begins sufficiently early; an *actual* signal would of course begin much earlier.

These considerations guide us in the choice of initial values for the orbital elements. We first select a value for  $e_0$ , the orbital eccentricity at the time the gravitational waves enter the detector's frequency band. We then set  $p_0$  equal to

$$p_0 = \frac{1 - e_0^2}{(2\pi M f_{\min}/3)^{2/3}} \simeq 180.42(1 - e_0^2) \left(\frac{M_\odot}{M}\right)^{2/3}, \quad (12)$$

TABLE I. Duration of the gravitational-wave signal (in seconds) as a function of initial eccentricity  $e_0$ , for selected binary systems. The binaries are labelled by the value of their individual masses, given in units of the solar mass. The missing entries correspond to binaries evolving too fast to give a useful gravitational-wave signal.

$e_0$	1.0 + 1.0	1.4 + 1.4	1.4 + 2.5	1.4 + 5.0	1.4 + 10	3.0 + 6.0	6.0 + 6.0	8.0 + 8.0
0.00	137.97	78.75	49.24	29.04	17.60	12.65	6.96	4.31
0.05	136.71	77.94	48.81	28.78	17.42	12.53	6.90	4.26
0.10	133.02	75.90	47.48	28.01	16.95	12.19	6.70	4.15
0.15	126.99	72.49	45.32	26.73	16.19	11.64	6.41	3.96
0.20	118.91	67.89	42.44	25.04	15.16	10.90	6.00	3.71
0.25	110.15	62.31	38.95	22.98	13.92	10.00	5.50	3.40
0.30	98.03	55.95	34.99	20.63	12.50	8.99	4.94	3.06
0.35	86.06	49.10	30.71	18.12	10.97	7.89	4.34	2.68
0.40	73.65	42.05	26.29	15.50	9.38	6.75	3.71	2.29
0.45	61.28	34.97	21.87	12.89	7.81	5.62	3.08	–
0.50	49.37	28.18	17.63	10.39	6.28	4.52	2.49	–
0.55	38.31	21.86	13.67	8.06	4.88	3.51	–	–
0.60	28.41	16.21	10.15	5.97	3.61	–	–	–
0.65	19.95	11.38	7.12	–	–	–	–	–

so that  $f_{\text{orb}} = f_{\text{min}}/3$  at the initial moment. The choice of initial value for the orbital phase is inconsequential, and we simply set  $\Phi_0 = 0$ .

In practice, Eqs. (6), (8), and (9) must be integrated numerically. We do so with the help of the Bulirsch-Stoer method (*Numerical Recipes* [26], Sec. 16.4). The functions  $p(t)$ ,  $e(t)$ , and  $\Phi(t)$  are tabulated (at nonuniform time intervals selected by the routine’s adaptive stepsize controller), and cubic spline interpolation (*Numerical Recipes*, Sec. 3.3) is used to evaluate them away from the tabulated points. In this way we construct the waveform  $s(t)$ , which is displayed in Fig. 2 for a specific choice of binary system.

The Newtonian approximation does not provide a natural cutoff for the waveforms. Equations (8) and (9) predict that the orbital frequency increases all the way to infinity, but this prediction is unphysical. A relativistic calculation shows instead that the inspiral proceeds up to a point of instability, from which the two companions undergo a catastrophic plunge toward each other. The exact moment of instability is still poorly determined, even in the case of circular orbits [27–29]. As a crude way of cutting off our waveforms, we simply stop the integration of the orbital equations at a time  $t_{\text{max}}$  such that  $p \gtrsim 6$ . (For a test mass moving in the gravitational field of a Schwarzschild black hole,  $p = 6$  designates the innermost stable circular orbit.) Except for the very massive binaries, the orbit has essentially become circular by the time the system reaches the point of instability.

The values of  $t_{\text{max}}$  for selected binary systems are listed in Table I. Since we start the integration at  $t = 0$ , this corresponds to the total duration of the signal, from the time it enters the instrument’s frequency band to the estimated point of instability. The Table reveals two important trends. First, for a given selection of masses, the signal duration *decreases* with increasing initial eccentricity. Second, for a given initial eccentricity, the



signal duration *decreases* as the mass of the system increases. Both trends can be understood by combining Eq. (8), evaluated at  $t = 0$ , with Eq. (12). This gives  $|dp/dt|_0 \propto \mu f_{\min}^2 (1 - e_0^2)^{-3/2} (1 + \frac{7}{8}e_0^2)$ , which states that increasing either  $e_0$  or  $\mu$  produces a larger initial  $|dp/dt|$ , and therefore a faster evolution.

### III. NONOPTIMAL PROCESSING OF ECCENTRIC SIGNAL

We imagine a detection strategy in which it was decided ahead of time that the expected signals would come from fully circularized binaries. The strategy, based on matched filtering, employs a bank of circular templates  $h(t; \boldsymbol{\theta})$ . Supposing that some of the signals come from eccentric binaries, we wish to calculate how much signal-to-noise ratio is lost when searching for them with nonoptimal filters. As was explained in Sec. I, this is given by the fitting factor, defined in Eq. (4).

We use the Newtonian approximation to construct the templates. They can be expressed directly in the frequency domain as [1]

$$\tilde{h}(f; \boldsymbol{\theta}) = A(f/f_0)^{-7/6} e^{i(2\pi f t_c - \phi_c)} e^{i\psi(f)}, \quad (13)$$

where  $A$  is an amplitude parameter,  $t_c$  a time-of-arrival parameter, and  $\phi_c$  a phase-at-arrival parameter. Also,  $f_0$  was defined in Eq. (3), and

$$\psi(f) = \frac{3}{128} (\pi \mathcal{M} f)^{-5/3}, \quad (14)$$

where  $\mathcal{M}$  is the chirp-mass parameter. Because  $A$  plays no role in the calculation of the fitting factor, we set  $A = 1$  and take  $\boldsymbol{\theta} = (t_c, \phi_c, \mathcal{M})$ . If the binary system were truly circular, then these parameters would have a clear physical meaning; for example, the chirp mass would be given in terms of the individual masses by [1]

$$\mathcal{M}_{\text{actual}} \equiv \frac{(m_1 m_2)^{3/5}}{(m_1 + m_2)^{1/5}}. \quad (15)$$

Our binaries, however, are not circular, and we shall treat  $t_c$ ,  $\phi_c$ , and  $\mathcal{M}$  as phenomenological parameters with no direct physical relevance. The issue at stake here is whether the templates of Eq. (13) are effective at searching signals from eccentric binaries.

The Fourier transform of the circular waveforms  $h(t, \boldsymbol{\theta})$  can be calculated accurately on the basis of the stationary-phase approximation [30]; this calculation leads to Eq. (13) above. This approximation, however, is not useful for eccentric waveforms, because the instantaneous orbital frequency  $d\Phi/dt$  is not a monotonic function of time. We therefore calculate  $\tilde{s}(f)$  by fast Fourier transform (*Numerical Recipes* [26], Sec. 12.2). Because  $s(t)$  contains three frequency components (at once, twice, and three times the orbital frequency), the Fourier transform of an eccentric signal displays more structure than that of a circular signal. This is illustrated in Fig. 3, which shows the emergence of the three frequency components in  $|\tilde{s}(f)|$ , as well as the interference between them.

We now describe the calculation of the ambiguity function and its maximization over the template parameters. The overlap integral between signal and templates can be written as

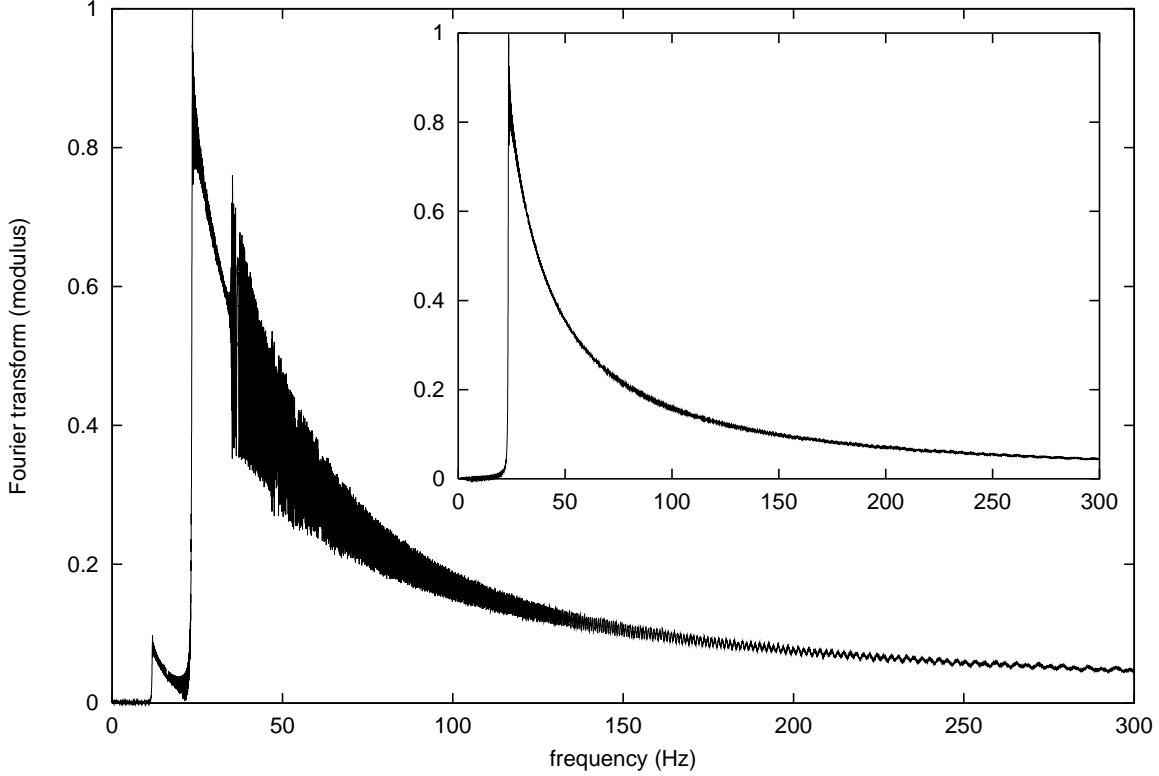


FIG. 3. Plots of  $|\tilde{s}(f)|$  for a 1.4 + 1.4 binary system. The main figure shows the Fourier transform of a signal with initial eccentricity  $e_0 = 0.1$ . As explained in the text, the signal is taken to start abruptly when  $f_{\text{orb}} = 13.3$  Hz, which explains the (artificial) cutoffs at low frequency. The three components of the gravitational-wave signal, and the interference between them, are clearly apparent. For comparison, the inset shows the Fourier transform of a circular signal, which also starts abruptly when  $f_{\text{orb}} = 13.3$  Hz.

$$(s|h) = 2 \left[ e^{i\phi_c} \mathcal{B}(t_c, \mathcal{M}) + e^{-i\phi_c} \mathcal{B}^*(t_c, \mathcal{M}) \right], \quad (16)$$

where

$$\mathcal{B}(t_c, \mathcal{M}) = \int_0^\infty \frac{(f/f_0)^{-7/6} e^{i\psi} \tilde{s}(f)}{S_n(f)} e^{-2\pi i f t_c} df. \quad (17)$$

We note that  $(h|h)$  is independent of  $\phi_c$  and  $t_c$ , so that maximization of the ambiguity function over these parameters is achieved by maximizing  $(s|h)$  alone. Maximization over  $\phi_c$  is straightforward, and we obtain

$$\max_{\phi_c} (s|h) = 4 |\mathcal{B}(t_c, \mathcal{M})|. \quad (18)$$

The integral of Eq. (17) is naturally evaluated by fast Fourier transform. For a given value of  $\mathcal{M}$ , this returns a discretized version of the function  $\mathcal{B}(t_c)$ . Maximization over  $t_c$  is achieved simply by selecting the largest value of  $|\mathcal{B}(t_c)|$ , which we denote  $|\mathcal{B}|_{\text{max}}$ . These manipulations give us a reduced ambiguity function,

$$\mathcal{A}(\mathcal{M}) \equiv \max_{t_c, \phi_c} \mathcal{A}(t_c, \phi_c, \mathcal{M}) = \frac{4 |\mathcal{B}|_{\text{max}}}{\sqrt{(s|s)(h|h)}}, \quad (19)$$

TABLE II. Fitting factor as a function of initial eccentricity  $e_0$ , for selected binary systems. Two independent numerical codes were written to calculate these numbers. The results differ by less than 1%, and we take this to be an estimate of our numerical accuracy.

$e_0$	1.0 + 1.0	1.4 + 1.4	1.4 + 2.5	1.4 + 5.0	1.4 + 10	3.0 + 6.0	6.0 + 6.0	8.0 + 8.0
0.00	0.998	0.997	0.999	0.998	0.998	0.998	0.998	0.999
0.05	0.960	0.976	0.985	0.992	0.992	0.998	0.996	0.996
0.10	0.898	0.931	0.947	0.965	0.976	0.984	0.993	0.993
0.15	0.836	0.879	0.902	0.930	0.946	0.961	0.975	0.987
0.20	0.762	0.822	0.854	0.893	0.913	0.934	0.955	0.973
0.25	0.695	0.761	0.802	0.852	0.885	0.903	0.930	0.952
0.30	0.630	0.637	0.749	0.805	0.850	0.868	0.900	0.925
0.35	0.569	0.581	0.693	0.753	0.811	0.829	0.867	0.893
0.40	0.513	0.520	0.635	0.698	0.765	0.783	0.827	0.854
0.45	0.454	0.460	0.574	0.637	0.714	0.732	0.781	–
0.50	0.397	0.402	0.513	0.576	0.656	0.675	0.728	–
0.55	0.348	0.350	0.452	0.513	0.595	0.614	–	–
0.60	0.297	0.303	0.396	0.452	0.534	–	–	–
0.65	0.257	0.231	0.344	–	–	–	–	–

in which  $(s|s)$  is evaluated as a discrete sum using the fast Fourier transform of  $s(t)$ , and  $(h|h)$  is evaluated by Romberg integration (*Numerical Recipes* [26], Sec. 4.3).

The fitting factor is obtained by finding the maximum of  $\mathcal{A}(\mathcal{M})$ . We first sketch this function by evaluating the right-hand side of Eq. (19) for several values of  $\mathcal{M}$ . We observe that the maximum always occurs in the interval  $1.0 < \mathcal{M}/\mathcal{M}_{\text{actual}} < 1.2$ . Having thus bracketed the maximum, we find its position by golden-section search (*Numerical Recipes* [26], Sec. 10.1).

Table II contains our main results: It lists, for selected binary systems, the fitting factor as a function of  $e_0$ , the initial orbital eccentricity. We estimate the accuracy of our results to be within 1%. Plots of the fitting factor were presented in Fig. 1, and a discussion of our results can be found at the end of Sec. I. In Table III we list the values of the ratio  $\mathcal{M}/\mathcal{M}_{\text{actual}}$  that maximizes  $\mathcal{A}(\mathcal{M})$ . We see that the circular templates attempt to compensate for orbital eccentricity by overestimating the chirp-mass parameter. This was to be expected, because increasing the chirp mass produces a faster orbital evolution, which is also an effect of increasing the eccentricity.

#### IV. CONCLUSION

The message of Table II and Fig. 1 is clear: Searching for eccentric signals with circular templates produces a loss of signal-to-noise ratio that increases with increasing eccentricity. We recall that the fitting factor is a measure of this loss of signal-to-noise ratio:  $\text{FF} = \text{SNR}|_{\text{actual}}/\text{SNR}|_{\text{optimal}}$ , where  $\text{SNR}|_{\text{actual}}$  is the signal-to-noise ratio obtained with nonoptimal (circular) templates, while  $\text{SNR}|_{\text{optimal}}$  is the signal-to-noise ratio that would be obtained if optimal (eccentric) templates were used instead. This is given by

TABLE III. Value of  $\mathcal{M}/\mathcal{M}_{\text{actual}}$  that maximizes the reduced ambiguity function.

$e_0$	1.0 + 1.0	1.4 + 1.4	1.4 + 2.5	1.4 + 5.0	1.4 + 10	3.0 + 6.0	6.0 + 6.0	8.0 + 8.0
0.00	1.0000	0.9999	0.9999	0.9999	0.9997	0.9997	0.9994	0.9992
0.05	1.0007	1.0006	1.0007	1.0007	1.0007	1.0006	1.0004	1.0005
0.10	1.0012	1.0016	1.0017	1.0022	1.0030	1.0031	1.0033	1.0036
0.15	1.0024	1.0027	1.0031	1.0039	1.0053	1.0056	1.0076	1.0094
0.20	1.0037	1.0042	1.0048	1.0060	1.0083	1.0083	1.0113	1.0160
0.25	1.0059	1.0059	1.0071	1.0087	1.0122	1.0122	1.0165	1.0222
0.30	1.0088	1.0095	1.0106	1.0121	1.0172	1.0170	1.0228	1.0314
0.35	1.0125	1.0134	1.0149	1.0167	1.0234	1.0232	1.0312	1.0429
0.40	1.0182	1.0194	1.0210	1.0223	1.0319	1.0314	1.0418	1.0563
0.45	1.0260	1.0288	1.0302	1.0307	1.0430	1.0416	1.0562	–
0.50	1.0404	1.0412	1.0447	1.0466	1.0586	1.0574	1.0774	–
0.55	1.0598	1.0654	1.0640	1.0680	1.0842	1.0749	–	–
0.60	1.0986	1.0946	1.0986	1.0976	1.1138	–	–	–
0.65	1.1508	1.1542	1.1484	–	–	–	–	–

$$\text{SNR}|_{\text{optimal}} = \sqrt{(s|s)} \equiv \rho. \quad (20)$$

Another important piece of information is how  $\rho$  varies with  $e_0$ . Because an eccentric signal is essentially a superposition of three frequency components, while a circular signal contains a single component at twice the orbital frequency, we expect that  $\rho(e_0)$  should increase with increasing eccentricity. Figure 4 confirms this expectation by showing that the relative increase in signal-to-noise ratio, measured by  $\rho(e_0)/\rho(0)$ , is indeed an increasing function of  $e_0$ . (This means that an eccentric binary system located at a distance  $R$  from the detector produces a stronger signal than a circular system at the same distance.) The increase, however, is modest with respect to the decrease incurred by nonoptimal filtering. The net effect is still a decrease in signal-to-noise ratio.

It would be highly desirable to extend our results to other gravitational-wave detectors — such as the advanced version of LIGO — and to post-Newtonian waveforms. The advanced LIGO detector is characterized by a wider frequency band starting at  $f = 10$  Hz; because the circular templates must then stay in phase with the eccentric signal over a longer period, we would anticipate lower values for the fitting factor. However, the dependence of the fitting factor on initial eccentricity and binary mass should be qualitatively the same. On the other hand, we would anticipate that post-Newtonian waveforms will produce higher values for the fitting factor. The reason is that the waveforms now come with additional parameters, and the added flexibility in the maximization procedure will likely improve the overlap between signal and templates. An interesting question is whether the eccentric signals force the template parameters outside of their natural range. For example, the dimensionless reduced-mass parameter  $\eta = m_1 m_2 / (m_1 + m_2)^2$  is physically restricted to the interval  $\eta \leq \frac{1}{4}$ , but the value returned by the maximization procedure might exceed this limit. If this were the case, then a larger number of templates would be required in a search for eccentric binaries. We hope to return to these issues in a future publication.

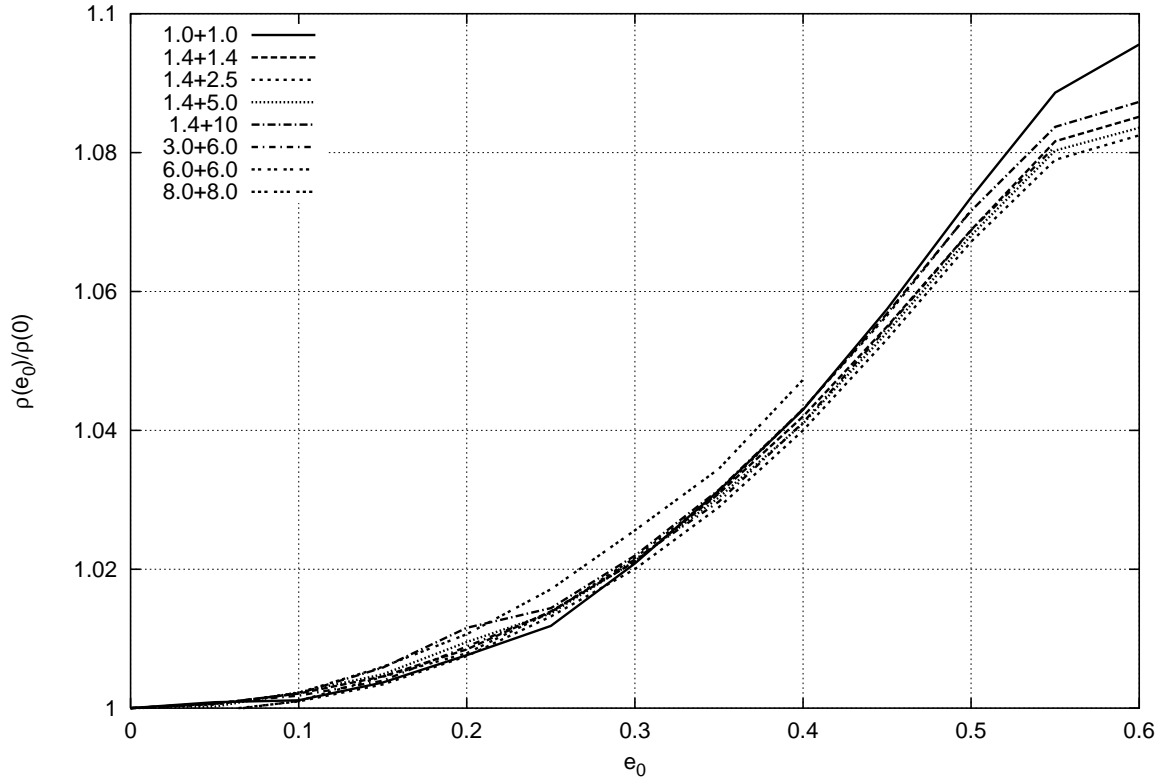


FIG. 4. The ratio  $\rho(e_0)/\rho(0)$  as a function of initial eccentricity, for selected binary systems. The scatter in the curves is mostly an artifact of numerical error.

#### ACKNOWLEDGMENTS

This work was supported by the Natural Sciences and Engineering Research Council of Canada. We thank Scott Hughes and an anonymous referee for their comments on a previous version of this manuscript.

## REFERENCES

- [1] K.S. Thorne, in *300 Years of Gravitation*, edited by S.W. Hawking and W. Israel (Cambridge University Press, Cambridge, England, 1987), p. 330.
- [2] B.F. Schutz, in *The Detection of Gravitational waves*, edited by D.G. Blair (Cambridge University Press, Cambridge, England, 1991), p. 406.
- [3] B.S. Sathyaprakash and S.V. Dhurandhar, Phys. Rev. D **44**, 3819 (1991).
- [4] S.V. Dhurandhar and B.S. Sathyaprakash, Phys. Rev. D **49**, 1707 (1994).
- [5] C. Cutler and É.É. Flanagan, Phys. Rev. D **49**, 2658 (1994).
- [6] R. Balasubramanian and S.V. Dhurandhar, Phys. Rev. D **50**, 6080 (1994).
- [7] B.S. Sathyaprakash, Phys. Rev. D **50**, 7111 (1994).
- [8] T.A. Apostolatos, Phys. Rev. D **52**, 605 (1996).
- [9] E. Poisson and C.M. Will, Phys. Rev. D **52**, 848 (1995).
- [10] R. Balasubramanian, B.S. Sathyaprakash, and S.V. Dhurandhar, Phys. Rev. D **53**, 3033 (1996).
- [11] B.J. Owen, Phys. Rev. D **53**, 6749 (1996).
- [12] T.A. Apostolatos, Phys. Rev. D **54**, 2421 (1996).
- [13] S. Droz and E. Poisson, Phys. Rev. D **56**, 4449 (1997).
- [14] T. Damour, B.R. Iyer, and B.S. Sathyaprakash, Phys. Rev. D **57**, 885 (1998).
- [15] R. Balasubramanian and S.V. Dhurandhar, Phys. Rev. D **57**, 3408 (1998).
- [16] E.E. Flanagan and S.A. Hughes, Phys. Rev. D **57**, 4535 (1998); 4566 (1998).
- [17] B.J. Owen and B.S. Sathyaprakash, Phys. Rev. D **60**, 022002.
- [18] B. Allen *et al.*, GRASP software package,  
<http://www.lsc-group.phys.uwm.edu/~ballen/grasp-distribution/>.
- [19] L.A. Wainstein and V.D. Zubakov, *Extraction of Signals from Noise* (Prentice-Hall, Englewood Cliffs, 1962).
- [20] P.C. Peters, Phys. Rev. **136**, B1224 (1964).
- [21] S.L. Shapiro and S.A. Teukolsky, Astrophys. J. **292**, L41 (1985).
- [22] G.D. Quinlan and S.L. Shapiro, Astrophys. J. **321**, 199 (1987).
- [23] L. Blanchet, B.R. Iyer, C.M. Will, and A.G. Wiseman, Class. Quantum Grav. **13**, 575 (1996).
- [24] A. Gopakumar and B.R. Iyer, Phys. Rev. D **56**, 7708 (1997).
- [25] H. Wahlquist, Gen. Relativ. Gravit. **19**, 1101 (1987).
- [26] W.H. Press, S.A. Teukolsky, W.T. Vetterling, and B.P. Flannery, *Numerical Recipes in C, Second Edition* (Cambridge University Press, Cambridge, England, 1992).
- [27] J.K. Blackburn and S. Detweiler, Phys. Rev. D **46**, 2318 (1992).
- [28] L.E. Kidder, C.M. Will, and A.G. Wiseman, Phys. Rev. D **47**, 3281 (1993).
- [29] G.B. Cook, Phys. Rev. D **50**, 5025 (1994).
- [30] S. Droz, D.J. Knapp, E. Poisson, and B.J. Owen, Phys. Rev. D **59**, 124016 (1999).